THE JOURNAL OF PHYSICAL CHEMISTRY B

Article

pubs.acs.org/JPCB

Preparation and Protein Immobilization of Magnetic Dialdehyde Starch Nanoparticles

Wensheng Lu,[†,‡] Yuhua Shen,*[,†] Anjian Xie,[†] and Weiqiang Zhang[†,‡]

[†]School of Chemistry and Chemical Engineering, Anhui University, Hefei 230039, P. R. China

[‡]Coordination Chemistry Institute, School of Chemistry and Chemical Engineering & Life Science, Chaohu University, Chaohu 238000, P. R. China

ABSTRACT: Superparamagnetic Fe_3O_4 nanoparticles were obtained using a hydrolysis product of starch, i.e., α-D-glucose, as the reducing agent and without any additional stabilizer and dispersant by a facile and green method at mild temperature. Magnetic dialdehyde starch nanoparticles (MDASN) were successfully synthesized with dialdehyde starch (DAS) as wrapper and epichlorohydrin as cross-linker by coembedding method. Bovine serum albumin (BSA) as a model drug was immobilized on the suface of MDASN. The particle size distribution of MDASN was 50−150 nm, and the average size was about 100 nm. The content of aldehyde group in DAS was 59.5%, and the package rate of DAS in MDASN was 33.2%. The loading amount and encapsulation efficiency of MDASN loading BSA were 5.0% and 54.4%, respectively. The saturation magnetization of MDASN at 300 K was 29.5 emu/g without coercivity and remanence. The as-prepared MDASN have not only lots of aldehyde functional groups but also stronger magnetic response, which might have potential applications such as drug carriers and targeted drug release.

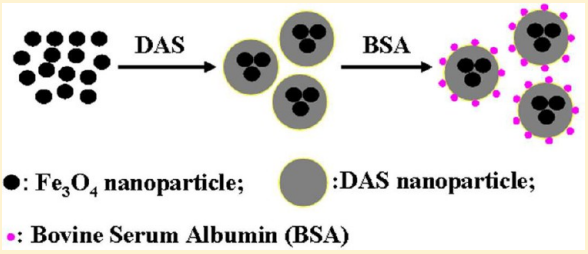

INTRODUCTION

Magnetic biomolecule composite nanomaterials are a kind of important biological material and have good biocompatibility and excellent targeting performance, which have potential applications as carriers of drugs, cells, and other biological materials or as magnetic target materials in biomedicine and other fields.[1−9] Their preparation and application have attracted extensive attention. Fe_3O_4 is one of the most commonly used magnetic nanoparticles; biological molecules have mainly carbohydrates, amino acids and proteins, carboxylic acid and its salts, esters, alcohols, and a few of the nucleic acids, etc.[10−18]

Starch is a green renewable resource and has good biocompatibility and nonimmunogenicity, which is the most commonly used drugs filler in the field of medicine.[19,20] Modified starch with heterogeneous nature and different applications can be obtained by physical or chemical methods or biological degradation.[21,22] Dialdehyde starch (DAS) is one kind of modified starch, using starch as raw materials, periodic acid, or periodate as oxidant so as to oxidize 2,3 -*o*-dihydroxy of the starch to dialdehydes. Dialdehyde starch has many excellent physical, chemical, biochemical characteristics, such as alkali solubility, easy cross-linking branches, strong bonding and other properties, and good safety, biological degradation, chemical activity, and wide applications in addition to containing many aldehyde functional groups.[23−28]

Herein, we have reported a facile method to synthesize magnetic dialdehyde starch nanoparticles (MDASN) with α-D-glucose obtained by hydrolysis of starch in acidic chloride ferric solution as the reductant, $NH_3{\cdot}H_2O$ as precipitating agent, sodium periodate as oxidant, DAS as wrapper, and epichlorohydrin as cross-linking agent. An amount of starch was first added to aqueous solution containing 0.3 M Fe^{3+} to adjust the ratio of Fe^{2+}/Fe^{3+} for 1:2. Second, DAS was prepared with soluble starch as raw material, sodium periodate as oxidant to transform the hydroxyl group into the aldehyde group with stronger chemical activity for reaction with alcohols, acids, amines, hydrazine, imine, and so on. Finally, MDASN were synthesized by adding DAS to the solution containing Fe_3O_4 nanoparticles with epichlorohydrin as cross-linking agent. On this basis, we have also studied the drug-loading property of MDASN with bovine serum albumin (BSA) as model drug.

EXPERIMENTAL SECTION

Materials. All chemicals were analytical reagent grade and used without further treatment, and all solutions were prepared with doubly distilled water. Ferric chloride hexahydrate ($FeCl_3{\cdot}6H_2O$), starch $[(C_6H_{10}O_5)_x]$, sodium periodate ($NaIO_4$), $NH_3{\cdot}H_2O$ (25%, w/w), and epichlorohydrin (C_3H_5ClO) were all purchased from Shanghai Reagent Co., China. Bovine serum albumin (BSA, molecular weight 69 kDa) was purchased from Sigma Chemical Co.

Synthesis of Fe_3O_4 Magnetic Nanoparticles. Fe_3O_4 magnetic nanoparticles were synthesized without any additional stabilizer and dispersant according to the following procedure. First, 4.2 mL of 1% starch solution was added into 50 mL of aqueous solution containing 0.03 M Fe^{3+} under mechanical

Received: November 9, 2012
Revised: February 21, 2013
Published: March 25, 2013

   dx.doi.org/10.1021/jp3110908 | J. Phys. Chem. B 2013, 117, 3720−3725

Table 1. Content of Aldehyde Group at Different Mass Ratios

sodium periodate:starch	C_1 (mol/L)	V_1 (mL)	C_2 (mol/L)	V_2 (mL)	G (g)	aldehyde content
0.5:1	0.25	5 + 2.8	0.22	7.5	0.104	0.460
0.7:1	0.25	5 + 3.1	0.22	7.5	0.101	0.595
0.9:1	0.24	5 + 3.4	0.21	7.5	0.101	0.700
1.1:1	*0.28*	*5 + 2.7*	*0.22*	*7.5*	*0.103*	*0.780*

stirring for a period of time at 90 °C. Second, the mixture solution was added dropwise into 30 mL of 5 M $NH_3{\cdot}H_2O$ solution at a constant of pH 10 under vigorous mechanical stirring (2000 rpm) for 30 min at 60 °C. The color of the suspension turned to black immediately. The suspension was cooled to room temperature, and the precipitated powders were separated from the suspension by applying an external magnetic field and washed three times with doubly distilled water and several times with ethanol. The supernatant solution was removed from the precipitate after decantation. Finally, Fe_3O_4 magnetic nanoparticles were dried in a vacuum oven at 60 °C for 12 h and stored in a stoppered bottle for further use.

Preparation of DAS. Sodium periodate solution (0.7 M, pH 1.5) was added to the soluble starch suspension according to a certain proportion under magnetic stirring, the reaction temperature was controlled at 40 °C, and the reaction time was 3 h. After the reaction was finished, DAS was precipitated by the addition of acetone and washed three times with doubly distilled water and with acetone, respectively. Finally, DAS was dried in a vacuum oven at 40 °C for 12 h.

The Fourier transform infrared spectroscopy (FT-IR) results of DAS showed that the characteristic vibration absorption peaks of the pyran ring at 758, 856, and 927 cm^{-1} in the starch disappeared and that the aldehyde characteristic peak appeared. The characteristic vibration peaks of C═O double bond in aldehyde group, 2931, 2910 cm^{-1}, the characteristic vibration peak of C−C single bond in the C−CHO, 1323 cm^{-1}, and the characteristics vibration peak of C−H single bond in the C−CHO, 776 cm^{-1}, appeared; these proved that DAS had been successfully prepared.

Determination of Aldehyde Group Content in DAS. Periodic acid and its salts can oxidize starch specifically, the hydroxyl groups on the C_2 and C_3 carbon atoms of the glucose unit were oxidized into aldehyde groups by IO_4^-, the carbon bond in C_2-C_3 was broken, and its degree of oxidation was expressed with dialdehyde content.

The determination methods of aldehyde content are the following: alkali consumption,[29] which has wide adaptability, strong anti-interference capability, simple operation; sodium borohydride reduction method,[30] which was limited because of the specialized device; and spectrophotometry of 2.4-dinitrophenylhydrazine (DNP),[31] which has poor reproducibility. Aldehyde group content in DAS was determined with alkali consumption method in this study. Its principle is that double aldehyde can occur in a Cannizzaro reaction in a molecule to determine the dialdehyde content with acid−base titration.

DAS (0.10 g) and NaOH solution (5.00 mL, 0.25 M) were accurately added into a 250 mL Erlenmeyer flask, and the flask was placed in the 70 °C water bath for 2 min to dissolve the sample. After rapid cooling of the flask with running water for 1 min, HCl solution (7.50 mL, 0.25 M) was accurately added and then 15.00 mL distilled water was added. Upon addition of 5 drops of phenolphthalein indicator, the end point was titrated with 0.25 M NaOH solution. Dialdehyde content was calculated with the following formula

$$\text{aldehyde group content} = \frac{C_1V_1 - C_2V_2}{G/160 \times 1000} \times 100\%$$

where C_1 (mol/L) is the concentration of NaOH solution, V_1 (mL) is the volume of NaOH solution, C_2 (mol/L) is the concentration of HCl solution, V_2 (mL) is the volume of HCl solution, G (g) is the mass of DAS, and 160 is the molecular wieght of repeated unit of DAS.

In the preparation of DAS, reaction time was 3 h, reaction temperature 40 °C, pH value 1.5, and sodium periodate concentration 0.7 M. The aldehyde content in the product was investigated by the control of the different mass ratio of sodium periodate and starch (Table 1).

As seen from Table 1, with increase of mass ratio of sodium periodate and starch, aldehyde group content increases under the given conditions. Dialdehyde starch was prepared at 0.7:1 of the mass ratio of sodium periodate, and starch was used for follow-up experiment. It can not only save the dosage of sodium periodate to reduce the experimental cost, it can also satisfy the requirements of aldehyde group content (59.5%) in order to further conjugate with other substances, such as amine drugs.

Synthesis of MDASN. Fe_3O_4 nanoparticles (100.0 mg) prepared were dispersed in 50 mL of doubly distilled water by ultrasonic method, then 15 mL of 1% dialdehyde starch solution was added dropwise by ultrasonic dispersion for 5 min, and finally 1 μL of epichlorohydrin was added dropwise into the mixture solution under magnetic stirring for 6 h at 40 °C. The suspension was cooled to room temperature, and the precipitated powders were separated from the suspension by applying an external magnetic field and washed three times with doubly distilled water and several times with ethanol. MDASN were dried in a vacuum oven at 60 °C for 12 h and then stored in a stoppered bottle for further use.

Protein Loading of MDASN and Determination. First, 1.0% BSA mother liquid was prepared with 0.1 M phosphate buffer solution (PBS), and then BSA stock solution (100.00 mL, 0.1 mg/mL) was made. A series of concentrations (C) of standard solutions were prepared by adding 0.5, 1.0, 1.5, 2.0, 3.0, 4.0, 5.0, and 6.0 mL BSA stock solution into 10 mL volumetric flasks, respectively, and then volume metered with PBS. The absorbance (A) of BSA was measured at 280 nm by UV−visible spectrophotometer, and the linear regression equation was obtained from $A-C$ standard curve.

MDASN (20.0 mg) was added into 3.0 mL of 1.0% BSA mother liquor, and the mixture solution was placed in water bath shaker at 37 °C for 2 h. After the protein reached swelling equilibrium, the microspheres were washed repeatedly with doubly distilled water by applying an external magnetic field, were dried in a low-temperature drying vacuum oven, and then were stored at low temperature for further use.

The microspheres of MDASN loading BSA weighed accurately (2.0 mg) were added into hydrochloric acid solution

dx.doi.org/10.1021/jp3110908 | J. Phys. Chem. B 2013, 117, 3720−3725

(1.0 mL, 10 mmol/L) and soaked for 4 h, and then 4.0 mL of PBS was added. The mixture solution was shaken in a constant temperature water bath shaker at 37 °C for 24 h, and the supernatant liquid obtained by magnetic separation was measured to gain the total amount of BSA (i.e., BSA adsorbing and binding on the surfaces of the MDASN), based on the linear regression equation. Likewise, 2.0 mg of the microspheres was volume metered with PBS, the mixture solution was shaken in a constant temperature water bath shaker at 37 °C for 4 h, and the supernatant liquid was measured to obtain the free amount of BSA (i.e., BSA adsorbing on the surface of MDASN).

Protein loading and encapsulation efficiency of MDASN were calculated according to the following formulas:

$$\text{protein loading} = \frac{\text{the total amount of protein} - \text{the free amount of protein}}{\text{the mass of microspheres}} \times 100\%$$

$$\text{encapsulation efficiency} = \frac{\text{the total amount of protein} - \text{the free amount of protein}}{\text{the total amount of protein}} \times 100\%$$

Characterization. The prepared samples were characterized as follows. The powder X-ray diffraction (XRD) was performed on a MAP18XAHF instrument, with the X-ray diffractometer using Cu Kα radiation (λ = 1.540 56 Å) at a scan rate of 6.0000 deg/min to determine the crystalline phase, and the accelerating voltage and applied current were 40 kV and 30 mA, respectively. Transmission electron microscope (TEM) and high-resolution TEM (HRTEM) were obtained on JEM model 100SX and 2010 electron microscopes (Japan Electron Co.) and operated at accelerating voltages of 80 and 200 kV, respectively. Field emission scanning electron microscopy (FE-SEM) was taken on a field emission scanning electron microscope (Hitachi S-4800). The X-ray photoelectron spectrometry (XPS) analysis was carried out on an ESCALAB MKII instrument at a pressure greater than 10^{-6} Pa. The general scan C1s, O1s, and Fe2p core level spectra were recorded with Mg Kα radiation as the exciting source (photon energy = 1253.6 eV). Absorption spectra were recorded on a Perkin-Elmer Lambda 900 UV/vis/NIR spectrometer. The Fourier transform infrared spectroscopy (FT-IR) was measured on Nicolet NEXUS 870 infrared spectrometer with KBr pellet. The thermogravimetric analysis (TGA) was carried out on a TGA/DSC apparatus (Pyris-1, Perkin-Elmer, at a heating rate of 10 °C/min in flowing high-purity nitrogen gas with 20 mL/min). The magnetization of the samples was measured with a Quantum Design superconducting quantum interference device (SQUID) magnetometer (MPMS-XL-7) in the temperature range of 5−300 K. For zero-field-cooled (ZFC) and field-cooled (FC) experiments, the sample was cooled, and a constant field was applied during the warm scan.

RESULTS AND DISCUSSION

The TEM image in Figure 1a shows that the average size of as-synthesized Fe_3O_4 magnetite nanoparticles is ca. 15 nm with narrow size distribution. The HRTEM image (Figure 1b) indicates that the nanoparticles are structurally uniform with a lattice fringe spacing of ca. 0.25 nm, which corresponds well with the values of 0.253 nm of the (311) lattice plane of the cubic Fe_3O_4 (JCPDS card no. 75-1610). The morphologies and microstructure of as-prepared MDASN are investigated using TEM and FE-SEM. Figures 1c and 1d show that MDASN are

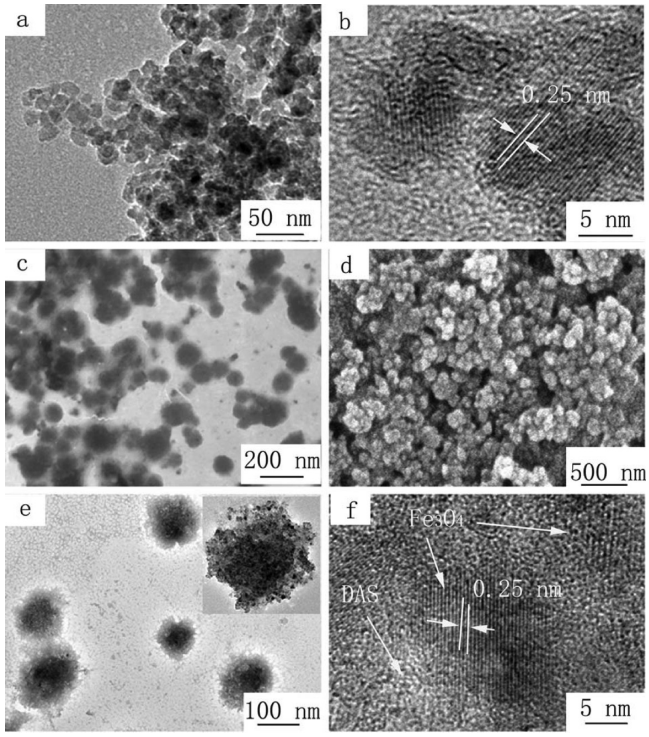

Figure 1. TEM image (a) and HR-TEM image (b) of as-synthesized Fe_3O_4 nanoparticles. TEM image (c), FE-SEM image, (d) and HR-TEM images (e, f) of as-prepared MDASN; the inset in (e) is a magnified picture of one MDASN.

spherical, and the average size is about 100 nm with 50−150 nm of the size distribution. As seen from Figures 1e and 1f, MDASN are multiphase structure. The deep color part is Fe_3O_4 nanoparticles, uniformly dispersed in the dialdehyde starch microspheres (Figure 1e). The lattice fringe (Figure 1f) is clear; the crystal plane spacing is about 0.25 nm, corresponding to the result of Figure 1b. The light color part is dialdehyde starch stained with phosphotungstic acid. The results preliminarily show that polymer composite nanoparticles of Fe_3O_4 coated with DAS have been successfully prepared, which were mainly based on the van der Waals force between DAS and magnetite nanoparticles.

The crystalline structure of the products was characterized by XRD. Figure 2 shows XRD patterns of as-prepared Fe_3O_4 nanoparticles (Figure 2a) and MDASN (Figure 2b). As shown in Figure 2a, the diffraction peaks at 2θ = 30.4°, 35.5°, 43.2°, 57.2°, and 62.9° can be well indexed to (220), (311), (400), (511), and (440) planes of the inverse cubic spinel structure of Fe_3O_4 (JCPDS card no. 75-1610), respectively, according to the reflection peak positions and relative intensities, which confirms the formation of the Fe_3O_4 nanoparticles. The main diffraction peaks of MDASN in Figure 2b can correspond to those of Fe_3O_4 in Figure 2a, which are significantly lower and broader. XRD results also confirm that Fe_3O_4 nanoparticles have well been coated by DAS and that MDASN have also been successfully obtained.

In order to further prove that the Fe_3O_4 nanoparticles are embedded in DAS particles, rather than adsorbed on the surface of DAS particles, the surface composition of MDASN can be measured through XPS. Figure 3 shows the energy spectra of the resulting products, in which the black curve is the full spectrum of Fe_3O_4 nanoparticles and the red one is the full

dx.doi.org/10.1021/jp3110908 | J. Phys. Chem. B 2013, 117, 3720−3725

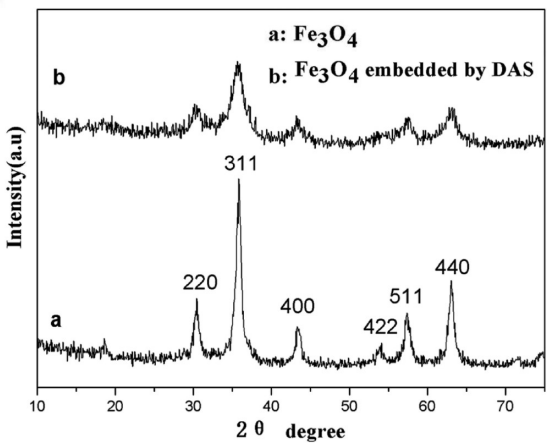

Figure 2. XRD patterns of as-synthesized Fe_3O_4 nanoparticles (a) and MDASN (b).

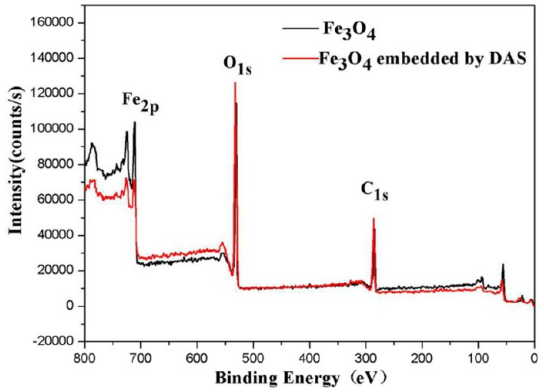

Figure 3. XPS of the products: black curve, Fe_3O_4 nanoparticles; red curve, MDASN.

spectrum of MDASN. As seen from the full spectra of energy spectra, absorption peaks of C1s (284.6 eV) and O1s (532.0 eV) of MDASN are significantly stronger than that of Fe_3O_4 nanoparticles, while absorption peaks of Fe2p (711.2 and 724.7 eV) of MDASN are significantly weaker than that of Fe_3O_4 nanoparticles. As we know, XPS mainly reveals the information of the surface with a depth of 0.1−10 nm. Thus it can be concluded that Fe_3O_4 nanoparticles are entrapped in DAS particles and not adsorbed on the surface of DAS particles. It is similar to the literature.[32]

Table 2 shows the analysis results of XPS of Fe_3O_4 and MDASN. By comparing the content and percentage of each

Table 2. XPS of Fe_3O_4 and MDASN

	Fe_3O_4 nanoparticles		MDASN	
name	atom %	PP atom %	atom %	PP atom. %
C1s	29.78	33.44	35.09	40.25
O1s	43.83	51.22	52.45	50.5
N1s	1.02	3.22	0.54	2.48
Fe2p	25.37	12.13	11.91	6.77

element of Fe_3O_4 with that of MDASN, it can be found that Fe atomic content and weight percentage is higher in pure Fe_3O_4, and C and O atomic contents and weight percentages increase in MDASN. This can explain that Fe_3O_4 nanoparticles in MDASN have been entrapped in DAS.

Figures 4a, 4b, and 4c show FT-IR spectra of DAS, MDASN, and Fe_3O_4 nanoparticles, respectively. The peaks at 2931, 2910,

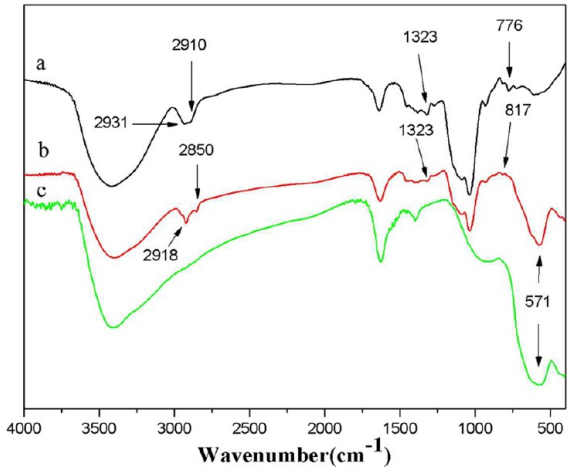

Figure 4. FT-IR spectra of the products: (a) dialdehyde starch; (b) MDASN; (c) Fe_3O_4 nanoparticles.

1323, and 776 cm^{-1} are the characteristic bands of aldehyde group in Figure 4a; the peak at 571 cm^{-1} is the characteristic peak of Fe_3O_4 (Figure 4c). The characteristic peaks of aldehyde group of MDASN are shifted (Figure 4b), which indicates that strong effect exists between DAS and Fe_3O_4 nanoparticles and that magnetic dialdehyde starch nanocomposite particles have been obtained.

Figure 5 shows the result of TGA on MDASN at the range of 20−700 °C under nitrogen atmosphere. As shown in Figure 5,

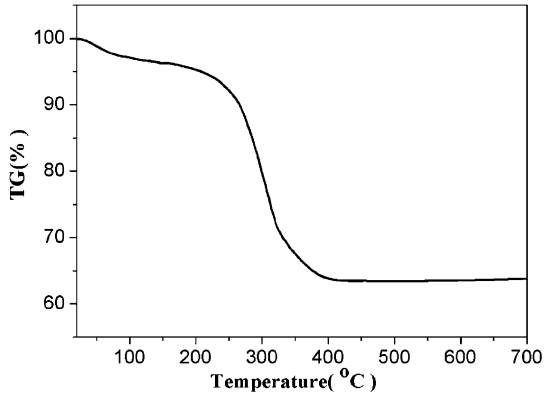

Figure 5. TG curve of MDASN.

there are two mass-loss processes before 500 °C. The mass-loss rates are about 3.5% and 33.2%, respectively. The first mass-loss process with the temperatures below 150 °C is due to the loss of water in MDASN, and the second mass-loss process between 200 and 500 °C is attributed to the thermal decomposition of dialdehyde starch composite nanoparticles. The TGA curve tends to level above 500 °C, which indicates that dialdehyde starch in magnetic composite nanoparticles has completely been decomposed and that the remnant is Fe_3O_4 nanoparticles. According to the results of TG, the contents of Fe_3O_4 and DAS in MDASN are 63.3% and 33.2%, respectively.

The magnetic properties of Fe_3O_4 and MDASN were measured by SQUID. Zero-field-cooled (ZFC) and field-cooled (FC) magnetization data measured with the field of 100 Oe in

dx.doi.org/10.1021/jp3110908 | J. Phys. Chem. B 2013, 117, 3720−3725

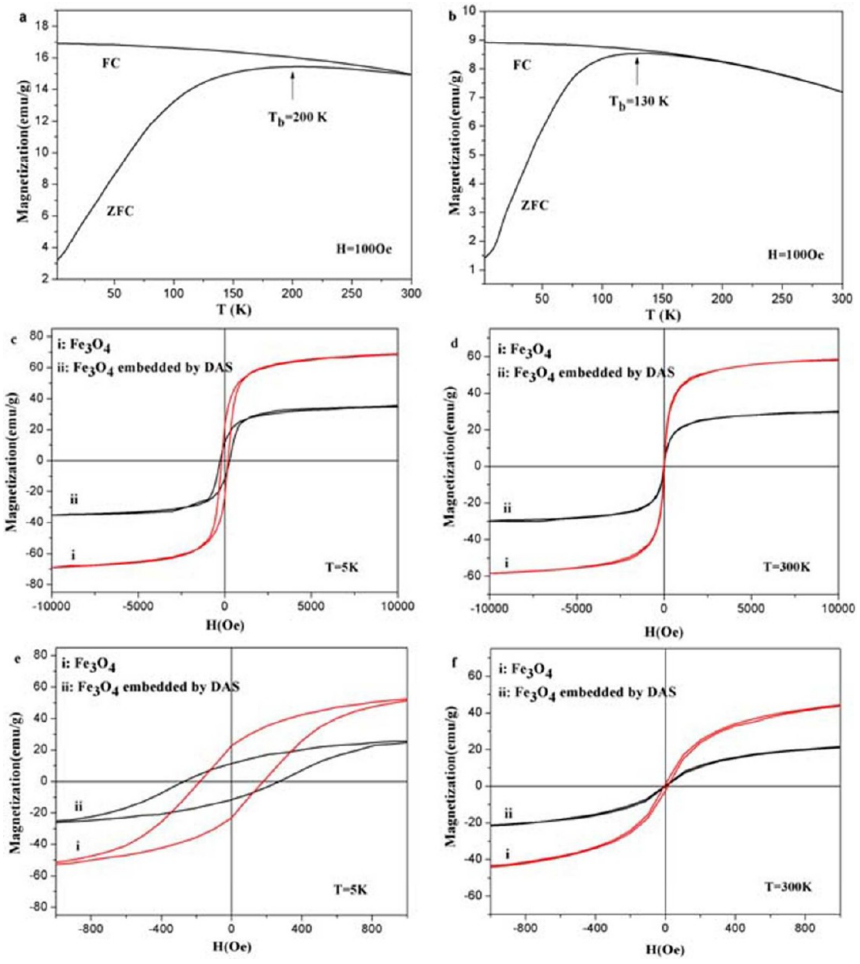

Figure 6. ZFC and FC curves of as-prepared Fe_3O_4 nanoparticles (a) and MDASN (b); magnetic hysteresis loops of Fe_3O_4 nanoparticles and MDASN at 5 K (c) and 300 K (d); (e) and (f) are magnified pictures of (c) and (d) at low field, respectively.

the temperature range of 2−300 K are shown in Figures 6a and 6b.

As seen from Figures 6a and 6b, blocking temperatures (T_b) of Fe_3O_4 and MDASN are 200 and 130 K, respectively. The latter is lower than the former, which shows that superparamagnetic property of MDASN is improved. Figures 6c and 6d are the hysteresis loops of Fe_3O_4 nanoparticles [Figures 6c (i) and 6d (i)] and MDASN [Figures 6c (ii) and 6d (ii)] at 5 and 300 K, respectively. Figures 6e and 6f are magnified pictures of Figures 6c and 6d at low field, respectively. As shown in Figures 6c and 6e, saturation magnetizations, remanences, and coercivitiess of Fe_3O_4 and MDASN are, respectively, 68.6 emu/g, 23.3 emu/g, and 183.4 Oe; 34.8 emu/g, 11.4 emu/g, and 275.7 Oe at 5 K at the field of 10 KOe, which confirms that the products are ferromagnetic below the blocking temperature.The hysteresis loops at 300 K (Figures 6d and 6f) show that saturation magnetizations of Fe_3O_4 and MDASN are, respectively, 58.1 and 29.5 emu/g at the field of 10 KOe, and the absence of coercivity and remanence indicates that the as-prepared Fe_3O_4 and MDASN have superparamagnetic properties above the blocking temperature.As seen from Figures 6c and 6d, the saturation magnetization of the MDASN is significantly lower than that of Fe_3O_4 nanoparticles, which is due to the presence of nonmagnetic dialdehyde starch, resulting in lower magnetism of unit mass in MDASN. But MDASN obtained still have a stronger saturation magnetization (29.5 emu/g), which also indicates that as-prepared products have potential applications as drug carriers and in targeted drug delivery.

As is known, the stability of aldehyde group in DAS at low pH is higher than that at high pH. In neutral or alkaline conditions, Schiff base can be formed via the nucleophilic addition reaction between the aldehyde group of DAS and the amino group of BSA. The loading capacity and entrapment efficiency of MDASN loading BSA were determined. On the basis of the relationship of the absorbance (A) of BSA at 280 nm and the concentration (C), the equation of linear regression is obtained as follows.

$$A = 0.00128 + 0.7032C, \quad R = 0.97843$$

The range of 0.005−0.06 mg/mL of BSA concentration shows a good linear relationship in accordance with the Lambert−Beer law (Figure 7).

According to the previous experiment, the total amount and free amount of protein of 2.0 mg of MDASN loading BSA are, respectively, 182.8 and 83.3 μg. The loading amount and encapsulation efficiency of MDASN loading BSA are 5.0% and 54.4%, respectively, which explains that the prepared MDASN have more powerful ability of loading and adsorption for protein. The adsorption mechanism of BSA on MDASN particles can be described as physical adsorption and covalent bonding between the carboxyl group of BAS and the aldehyde group of DAS.

dx.doi.org/10.1021/jp3110908 | J. Phys. Chem. B 2013, 117, 3720−3725

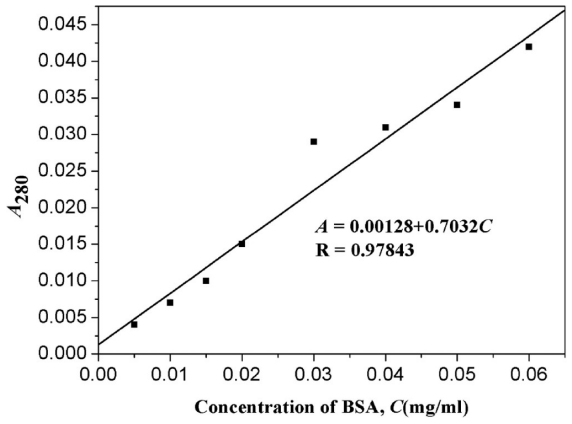

Figure 7. Standard curve of BSA.

■ CONCLUSION

In the study, superparamagnetic Fe_3O_4 nanoparticles and MDASN have been successfully prepared, and protein immobilization of MDASN with BSA as model has also been studied. The as-prepared MDASN have not only lots of aldehyde functional groups but also stronger magnetic response (saturation magnetization: 29.5 emu/g); thus, this study has established certain foundation for MDASN as targeted drug carriers.

■ AUTHOR INFORMATION

Corresponding Author

*E-mail: s_yuhua@163.com. Tel.: +86-551-5108090. Fax: +86-551-5108702.

Notes

The authors declare no competing financial interest.

■ ACKNOWLEDGMENTS

This work is supported by the National Natural Science Foundation of China (50973001, 31070730, and 21171001), the Provincial Natural Science Research Program of the Higher Education Institutions of Anhui Province, China (KJ2012A204), and the Doctoral Scientific Research Fund of Chaohu University, Chaohu, China.

■ REFERENCES

(1) Laurent, S.; Forge, D.; Port, M.; Roch, A.; Robic, C.; Vander Elst, L.; Muller, R. *Chem. Rev.* **2008**, *108*, 2064.
(2) Llandro, J.; Palfreyman, J. J.; Ionescu, A.; Barnes, C. H. W. *Med. Biol. Eng. Comput.* **2010**, *48*, 977.
(3) Ito, A.; Shinkai, M.; Honda, H.; Kobayashi, T. *J. Biosci. Bioeng.* **2005**, *100*, 1.
(4) Cheng, F. Y.; Su, C. H.; Yang, Y. S.; Yeh, C. S.; Tsai, C. Y.; Wu, C. L.; Wu, M. T.; Shieh, D. B. *Biomaterials* **2005**, *26*, 729.
(5) Qin, G. W.; Darain, F.; Wang, H.; Dimitrov, K. *J. Nanopart. Res.* **2011**, *13*, 45.
(6) Sunderland, C. J.; Steiert, M.; Talmadge, J. E.; Derfus, A. M.; Barry, S. E. *Drug Dev. Res.* **2006**, *67*, 70.
(7) Zhang, Y.; Zhang, J. *J. Colloid Interface Sci.* **2005**, *283*, 352.
(8) Choi, H.; Choi, S. R.; Zhou, R.; Kung, H. F.; Chen, I. W. *Acad. Radiol.* **2004**, *11*, 996.
(9) Jiang, J.; Gan, Z.; Yang, Y.; Du, B.; Qian, M.; Zhang, P. *J. Nanopart. Res.* **2009**, *11*, 1321.
(10) Roca, A. G.; Morales, M. P.; O'Grady, K.; Serna, C. J. *Nanotechnology* **2006**, *17*, 2783.
(11) Yan, F.; Zheng, X.; Sun, Z.; Zhao, A. *Polym. Bull.* **2011**, *68*, 1305.
(12) Guo, Z.; Shin, K.; Karki, A. B.; Young, D. P.; Kaner, R. B.; Hahn, H. T. *J. Nanopart. Res.* **2009**, *11*, 1441.
(13) Lu, W.; Shen, Y.; Xie, A.; Zhang, W. *J. Magn. Magn. Mater.* **2010**, *322*, 1828.
(14) Yang, Y.; Jiang, J.; Du, B.; Gan, Z.; Qian, M.; Zhang, P. *J. Mater. Sci.: Mater. Med.* **2009**, *20*, 301.
(15) Landmark, K. J.; DiMaggio, S.; Ward, J.; Kelly, C.; Vogt, S.; Hong, S.; Kotlyar, A.; Myc, A.; Thomas, T. P.; Penner-Hahn, J. E.; et al. *ASC Nano* **2008**, *4*, 773.
(16) Lu, W.; Shen, Y.; Xie, A.; Zhang, X.; Chang, W. *J. Phys. Chem. C* **2010**, *114*, 4846.
(17) Lu, S. L.; Ramos, J.; Forcada, J. *Langmuir* **2007**, *23*, 12893.
(18) Brahler, M.; Georgieva, R.; Buske, N.; Muller, A.; Muller, S.; Pinkernelle, J.; Teichgraber, U.; Voigt, A.; Baumler, H. *Nano Lett.* **2006**, *6*, 2505.
(19) Linda, S.; Lena, S.; Ingvar, S. *Vaccine* **2004**, *22*, 2863.
(20) Pohja, S.; Suihko, E.; Vidgren, M.; Paronen, P.; Ketolainen, J. *J. Controlled Release* **2004**, *94*, 293.
(21) Laura, T.; Eija, R.; Tarja, K.; Seppo, R.; Jukka, P.; Arto, U.; Soili, P.; Kristiina, J. *J. Controlled Release* **2004**, *98*, 407.
(22) Wikingsson, L. D.; Sjöholm, I. *Vaccine* **2002**, *20*, 3355.
(23) He, X.; Shen, B.; Liu, X. *Chin. J. Bioproc. Eng.* **2004**, *2*, 1.
(24) Wongsagona, R.; Shobsngobb, S.; Varavinita, S. *Starch* **2005**, *57*, 166.
(25) Para, A.; Stanislawa, K. K. *Carbohydr. Polym.* **2002**, *50*, 151.
(26) Tang, R.; Du, Y.; Fan, L. *J. Polym. Sci., Part B: Polym. Phys.* **2003**, *41*, 993.
(27) Wang, H.; Wei, R.; Shen, H. *Chin. J. Bioproc. Eng.* **2004**, *2*, 25.
(28) Onishi, H.; Nagai, T. *Int. J. Pharmaceut.* **1986**, *30*, 133.
(29) Hofreiter, B. T.; Alexander, B. H. *Anal. Chem.* **1955**, *27*, 1930.
(30) Rankin, J. C.; Mehltretter, C. L. *Anal. Chem.* **1956**, *28*, 1012.
(31) Wise, C. S.; Mehltretter, C. L. *Anal. Chem.* **1958**, *30*, 174.
(32) Wang, Z.; Guo, H.; Yu, Y.; He, N. *J. Magn. Magn. Mater.* **2006**, *302*, 397.